1.1 Conceptual uncertainties and their influence on bentonite hydration

Mattias Åkesson
Clay Technology AB, Lund, Sweden
November 2013

Contents

1 Introduction

1.1 Background

Conceptual uncertainties associated with thermal, hydraulic and mechanical processes in the near field of a repository has been investigated since many years, both theoretically and through large-scale experiments, in a number of EU projects and in the international DECOVALEX project (Tsang et al. 2009). This information has, according to the judgment by SSM, not been optimally utilized in the calculations of the re-saturation phase in SR-Site. SKB should analyze the relevance of the conclusions from other extensive experiments, such as FEBEX, and include a systematic analysis of conceptual uncertainties which can influence the modelling of the evolution of the re-saturation. It has for instance been suggested that the influence of thermo-osmotic effects and the occurrence of a threshold gradient has a significant influence (Sanchez et al. 2007) in particular for those longer re-saturation times which occur in SKB's case.

1.2 Scope

The aim of this analysis was: i) to give an overview of different experiments which have been used for modelling tasks; ii) to give an overview of conceptual uncertainties regarding the buffer re-saturation, which have been suggested in these modelling tasks; and iii) to evaluate the relevance of these uncertainties for the re-saturation calculations within SR-Site.

The analysis has above all focused on the large-scale experiments performed within the FEBEX project, and the modelling tasks which have addressed these experiments. A description of the FEBEX in-situ test is presented in Chapter 2, together with a summary of performed modelling tasks. The FEBEX mock-up test and the modelling tasks related to this test are summarized in Chapter 3. This chapter also includes descriptions of three non-standard flow models (threshold gradient in Darcy´s law, thermo-osmotic effects, and micro-fabric evolution) which have been analyzed within the framework of the modelling of FEBEX mock-up. An evaluation of the relevance of these non-standard flow models for the re-saturation calculations within SR-Site is presented in Chapter 4. Finally, in Chapter 5 a number of other uncertainties are described and evaluated.

2 FEBEX in-situ test

2.1 Test description

This section is based on information provided by Alonso and Alcoverro (2005) and Gens et al. (2009).

The FEBEX in-situ test has been performed (and is to some extent still running) in a granitic rock formation at the Grimsel test site in Switzerland. The FEBEX drift has a diameter of 2.28 m, and was excavated (using a TBM) in September - October 1995. The final 17.4 m of the drift was selected for the test.

The water inflow into the FEBEX drift was measured during January – May 1996, and was estimated to be 7.8 ml/min. This was found to be distributed among three types of water entry: 27% from matrix; 51% from well defined points; and the rest from fractures.

The mechanical installation was performed in July-October 1996. Two heaters (the outer and the inner were denoted Heater 1 and 2, respectively), with a diameter of 0.9 m and a length of 4.54 m, were installed within a buffer made of FEBEX bentonite blocks. The blocks had an initial water content of 14.4%, and an initial dry density of 1.7 g/cm^3. The overall dry density of the buffer, taking gaps into account, was 1.6 g/cm^3. The buffer was subjected to isothermal hydration during the first four months after the installation. The heating began on 27th February 1997. At first the heating was performed with constant power output, but on day 53 the system was switched to constant temperature mode, with a target temperature of 100 °C at the hottest point at the canister-bentonite contact. The heating from Heater 1 ended on 27th February 2002. The test was allowed to cool for 33 days, after which the outer half of the test was dismantled during a 75-days period. A new shotcrete plug was subsequently constructed, and the test of the remaining part of the experiment was continued.

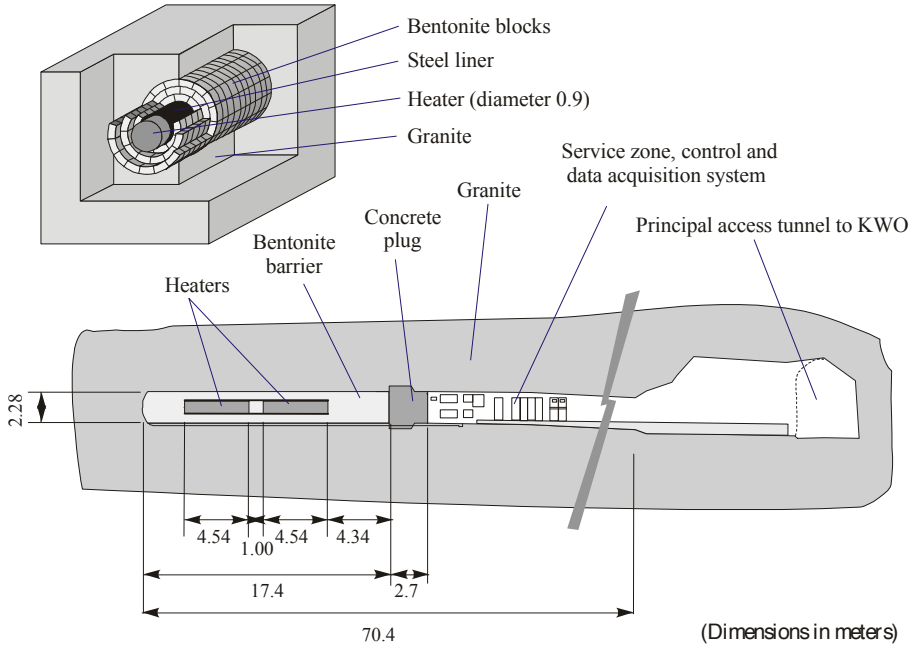

Figure 2-1. Overview of the FEBEX in-situ test.

2.2 Modelling performed within DECOVALEX

This section is based on information provided by Alonso and Alcoverro (2005) and Alonso et al. (2005).

The FEBEX in-situ test was selected as one of the modelling task (No 1) in the Decovalex III project which was carried out during 1999 to 2003. The modelling task was divided into three parts:

- A: HM modelling of the rock. The objective of this part was to predict the water inflow into the tunnel and the water pressure evolution in the rock during the tunnel excavation.
- B: THM analysis of the buffer behaviour. The objective of this part was to predict the evolution of the heating power, as well as the temperature, relative humidity and total stresses along selected sections and/or at specific points in the buffer during the first 1000 days of operation.
- C: THM analysis of the rock. The objective of this part was to predict the evolution of the temperature, water pressure, normal stress, radial displacement at specific points and/or along selected sections in the rock during the first 1000 days of operation.

Eight contributing teams presented modelling results for Part B (which is of main interest in this overview). A compilation of model features, couplings and some key factors used by the different teams are compiled in Table 2-1.

Table 2-1. Consideration of couplings and some key factors by the teams.

Team	Couplings	Dimens	Liq ↔ gas	Vap. flux	$k_w(S)$	$\lambda_T(S)$	$\varepsilon_v(s)$
BGR	TH→HM*	2			■		
CNS	THM	3	■	■	■		■
DOE	TH→TM	3	■	■	■	■	■
IPS	THM	1			■		
JNC	TH	3		■	■	■	
SKB	THM	2	■	■	■	■	■
SKI	THM	3	■	■	■	■	■
STU	TH	1	■	■	■	■	

Abbreviation	Physical phenomena
liq ↔ gas	Phase change between liquid water and water vapour
vap. Flux	Vapour flux
$k_w(S)$	Saturation-dependent water permeability
$\lambda_T(S)$	Saturation-dependent thermal conductivity
$\varepsilon_v(s)$	Suction-induced deformations

M* indicates that the mechanical reduces to consider a dependency on the swelling pressure.

The chosen time frame, i.e. the first 1000 days after the start of the heating, implied that the preceding and the subsequent time periods were excluded for modelling, and this had two consequences:

- The four months period with isothermal hydration, which followed the installation of the test, was included by some modelling teams, and this implied a better agreement with the experimental relative humidity (RH) data in the outer part of the test.

- The two year period, which followed the first 1000 days after the heating started, was not included in the models, and this meant that the models weren't compared with the data from the dismantling of the test.

A number of observations could be made from the presented predictions:

- **Thermal problem:** The temperature predictions varied significantly among the modelling teams, although the actual recorded values tended to remain at the average of all calculations. One observed feature was the initial reduction and the subsequent increase in the power required to maintain a constant temperature at the heater-buffer contact. This was an effect of the initial drying and the subsequent re-saturation of the inner part of the bentonite. Models which did not include a saturation-dependent thermal conductivity could not reproduce this effect, and only one of the predictions matched the actual behaviour correctly.

- **Hydraulic problem:** Models which included a correct TH coupling, (i.e. with representations of the liquid/vapour phase change; and the vapour flux) were capable of reproducing the observed evolution of relative humidity. This was specially the case for the predictions of the processes at the mid-section of the heaters. The processes in the central section of the test were, however, more complex and were not accurately reproduced by the models. Preferential vapour flow paths along open joints, which may have played a role in the FEBEX test, were not considered in the used models (a related process is described and assessed in section 5.2).

- **Mechanical problem:** Radial stresses recorded in the outer part of the buffer showed a continuous increase during the observation period and their value exceeded 3MPa at day 1000, whereas the pressure sensor located in the inner part of the buffer remained essentially unloaded during the same period. Some of the presented models predicted this distribution, while other models resulted in a more homogeneous build-up of stresses within the buffer.
  The porosity of the buffer remained constant in global terms due to the rigid confinement offered by the granite. The intrinsic permeability of the buffer could therefore be expected to be fairly constant. This implied that a correct prediction of the relative humidity evolution did not require a mechanical coupling. This was demonstrated by one of the modelling teams.

- **Influence of the rock matrix permeability:** Measurements of different RH distributions showed that the discrete conducting features of the rock had only a minor influence on the buffer hydration, and it was concluded that the low permeability of the saturated bentonite, ($1 \cdot 10^{-21}$ m^2) compared with the granite matrix permeability ($5 \cdot 10^{-19}$ m^2), leads to a fairly homogeneous hydration of the barrier. In other words, the bentonite permeability controlled its own rate of hydration and the rock matrix was capable of providing all the required flow of water.

2.3 Modelling of FEBEX in-situ test by UPC

After the completion of the FEBEX task within the Decovalex III project, Sánchez and Gens (2006) and Gens et al. (2009) presented results from a modelling work which encompassed the entire five year test period of the outer part of the experiment, which therefore also could include a comparison with data from the dismantling of that part. The model consisted of a 2D axisymmetric geometry, and employed the fully coupled thermo-hydro-mechanical formulation (including gas transport) as implemented in the Code_Bright FEM code. The heat transport was calculated with Fourier´s law, the advective transport of water and air followed Darcy´s law, and the diffusive transport of vapour followed Fick´s law. The used retention curve was a modification of the van Genuchten expression. For the mechanical behaviour a modified form of the Barcelona Basic Model was employed.

A number of observations could be made from a comparison of the model results and the data from the sensors in the bentonite:

- Thermal problem: The model was able to reproduce the temperature evolution generally well, although the calculated heating power was under-predicted by approximately 10 and 18%, for Heater 1 and 2, respectively.
- Hydraulic problem: The model was able to reproduce the evolution of RH very satisfactory. The outer part of the bentonite displayed a monotonic increase of RH, reflecting the hydration from the rock. In the inner part, however, the RH first displayed an increase, which reflected a vapour front from even warmer parts. This was immediately followed by drying with decreasing RH. Finally, the RH exhibited a slow increasing trend, also reflecting the hydration from the rock.
- Mechanical problem: The model was able to resemble the general build-up of total stresses and also the final value for a number of sensors. The relatively slow build-up of stresses in the inner part of the bentonite was, however, not reproduced.

The model also simulated the cooling stage and the excavation performed prior to sampling, and the model results could be compared with data from the analyses that were performed on samples obtained during the dismantling operation:

- Water content profiles: The numerical analysis showed very good agreement with the measured profiles of the water content. In sections close to the heater, the water content was still below the initial value. In cool sections, however, there was a small net gain in the central part of the tunnel. Close to the rock wall, in contrast, the water content had increased significantly.
- Dry density profiles: The numerical analysis also showed very good agreement with the measured profiles of the dry density. Close to the rock the bentonite had expanded, exhibiting dry density values well below the initial value. In contrast, in zones near the heater and in the central part of the tunnel, the dry density had increased.

It was concluded from this modeling work that the used THM formulation was able to capture the phenomena involved as well as their interactions, and also that it has a good predictive power. It was, however, also stated that it is possible that other phenomena may start playing a more significant role (such as thermo-osmosis, chemical effects, or the double porosity fabric of the compacted bentonite) when longer periods are considered.

3 FEBEX mock-up test

3.1 Test description

This section is based on information provided by Martin and Barcala (2005) and Sánchez and Gens (2006).

The FEBEX mock-up test has been performed and is still running in the laboratory of Ciemat in Madrid. The test is performed in a cylindrical steel body with a useful length of 6 m and an inner diameter of 1.62 m. Two heaters with a length of 1.62 m and a diameter of 0.34 m were installed within a buffer made of FEBEX bentonite blocks. The blocks had an initial water content of 13.6%, and an initial dry density of 1.77 g/cm^3. The overall dry density of the buffer, taking gaps into account, was 1.65 g/cm^3.

The experiment is equipped with an artificial hydration system by which granitic water has been used for hydration of the bentonite. Three days before the start of the test, a volume of 634 litres was injected in order to flood all the voids in gaps in the experiment. The heating and the hydration began simultaneously on 4th February 1997. At first the heating was performed with constant power output, but on day 10 the system was switched to constant temperature mode, with a target temperature of 100 °C at the heater-bentonite interface. The outer thermal boundary is set by the external climate which is maintained with air-conditioning at 20 ± 2 ºC. The water injection pressure has been between 0.5-0.6 MPa since the start.

An over-heating event occurred on day 1391 and lasted for 40 hours. The maximum temperature in the bentonite reached 240 ºC during this event.

From approximately day 900, the water uptake of the test has been significantly slower than what has been predicted, and this has motivated investigations of non-standard flow models (see next section). The slow water uptake coincided with a levelling out and even reduction of total stresses. An alternative explanation that a problem in the hydration system could affect the water supply to the bentonite has also been considered. However, according to Sánchez and Gens (2006), investigations have confirmed that there was no obstruction in the hydration system or geotextile, and that the water intake was nearly uniform over the entire hydration front.

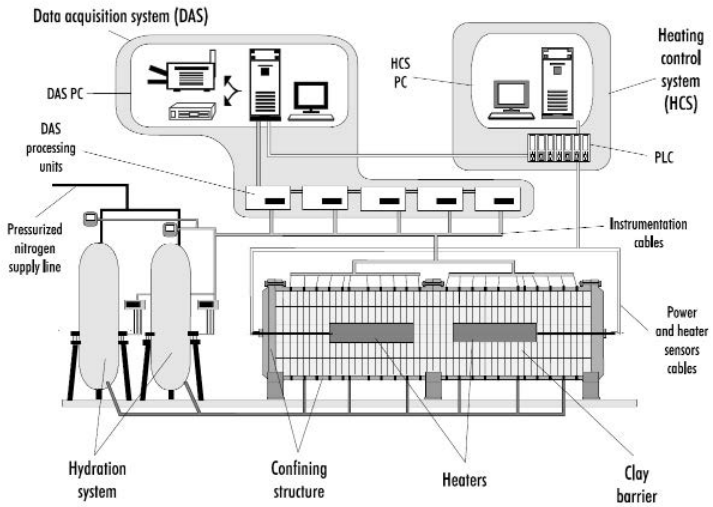

Figure 3-1. General layout of the FEBEX mock-up test.

3.2 Modelling of FEBEX mock-up test by UPC

Sánchez and Gens (2006) have presented results from a modelling work and compared this with experimental data from the operational stage with hydration and heating up to day 2417. In addition, results from a long-term (20 years) prediction were presented.

The model consisted of a 2D axisymmetric geometry, and employed the fully coupled thermo-hydro-mechanical formulation, as implemented in the Code_Bright FEM code and very similar the one used for the in-situ test model (section 2.3). The heat transport was calculated with Fourier´s law, the advective transport of water and air followed Darcy´s law, and the diffusive transport of vapour followed Fick´s law. The used retention curve was a modification of the van Genuchten expression. For the mechanical behaviour a modified form of the Barcelona Basic Model (Alonso et al. 1990) was employed.

A comparison of results from a base case model and the data from the sensors in the bentonite showed that:

- Thermal problem: The model was able to reproduce the temperature evolution generally well.
- Hydraulic problem: The model was able to reproduce the cumulative water-uptake and evolution of RH quite well up to day 900. After that the model tended to over-estimate the hydration rate.
- Mechanical problem: The model was able to resemble the general build-up of total stresses up till day 900. After that the model tended to over-estimate the build-up of stresses.

The observed differences concerning the hydration rate motivated the investigation of a number of non-standard flow models. These analyses were performed with 1-D axis-symmetrical models. Two characteristic sections were considered: one represented a section in the central part of the heaters and was modelled with a temperature of 100 ºC at the inner boundary, and one cold section representing the outer parts of the test was modelled with a temperature of 27 ºC at the internal part of the barrier. These investigations are summarized in the following subsections.

3.2.1 Threshold gradient

Darcy's law describes a linear relationship between the flux and the hydraulic gradient, and this law is generally valid at low Reynolds numbers (Bear 1972). Some authors have, however, discussed a lower limit for the applicability of Darcy's law (see for instance Bear (1972) and Mitchell (1993)), and such a lower limit would imply that a threshold gradient must be exceeded before any flow can be initiated (see Figure 3-2).

In the modelling of the FEBEX mock-up test, (Sánchez and Gens 2006), the following non-linear relationships between the flux and the hydraulic gradient were investigated:

- A threshold gradient (J_o) equal to 50
- A critical gradient (J_c) close to 2000.
- A power law for the range of hydraulic gradient with non-Darcian's flow.

It was found that a 1D axisymmetric THM model which included this description could capture the reduction in the hydration rate observed in the mock–up test. It was, however, also noted that the used approach implied that the barrier did not reach full water saturation.

The influence of a threshold gradient was also investigated in a model of one of the FEBEX infiltration test (Sanchez et al. 2007). In this case the used threshold gradient was also set to 50, while the critical gradient was set to a value close to 1500.

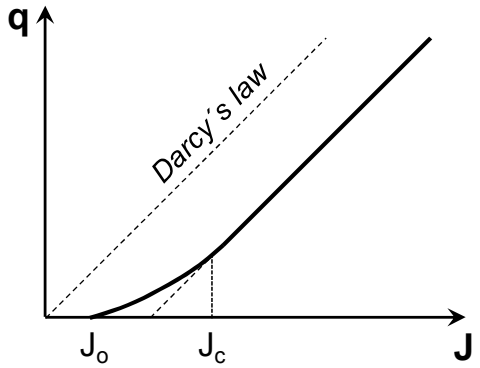

Figure 3-2. Linear and non-linear relationships between flux (q) and hydraulic gradient (J).

3.2.2 Thermo-osmosis

With thermo-osmosis is generally meant fluid flow which is caused by a temperature gradient. Such a coupled flow phenomena is supported by non-equilibrium thermodynamics (DeGroot and Mazur 1984, Mitchell 1993) and is one of several coupled flow phenomena which can occur, see Table 3-1.

In the modelling of the FEBEX mock-up test, (Sánchez and Gens 2006), the following equation was formulated in order to include the thermo-osmotic effect:

$$\mathbf{q}_l = -\mathbf{K}_{HH}(\nabla P_l - \rho_l \mathbf{g}) - \mathbf{K}_{HT}\nabla T \qquad (3\text{-}1)$$

The flow coefficient $\mathbf{K_{HH}}$ corresponds to $\mathbf{k}\cdot k_r/\mu$ used in Darcy's law, while $\mathbf{K}_{HT}$ is the phenomenological coefficient associated to the thermo-osmotic flow. For the FEBEX bentonite there were no experimental data, and for the modeling of the FEBEX mock-up a thermo-osmotic constant of $2.73\cdot10^{-13}$ $m^2/K/s$ was adopted, and this value was within the range of possible values found in the literature.

It was found that a 1D axisymmetric THM model which included this description displayed a somewhat better agreement with the RH evolution in the hot section close to the heater, but the overall tendency of the model could not be considered good. The measured trend in zones near the hydration front was not so well captured, and results from the model of the outer cold section were not influenced by the thermo-osmotic effect. It was also observed that it would be possible that the clay never reaches full saturation in the hot sections if this approach is used.

Sanchez et al (2007) also investigated thermo-osmosis in a model of the FEBEX infiltration test. In this case, the used thermo-osmotic constant was set to $5 \cdot 10^{-12}$ $m^2/K/s$. Finally, Zheng and Samper (2008) investigated thermo-osmosis in a model of the FEBEX mock-up, in which case the used thermo-osmotic constant was set to $3.62 \cdot 10^{-12}$ $m^2/K/s$.

Table 3-1. Direct and coupled flow phenomena.

	Gradients		
Flow	Hydraulic head	Chemical concentration	Temperature
Fluid	Darcy´s law	Chemical osmosis	Thermo osmosis
Ion	Streaming current	Fick´s law	Soret effect
Heat	Isothermal heat transfer	Dufour effect	Fourier´s law

3.2.3 Micro-fabric evolution

The notion of micro-fabric evolution is generally based on the following concepts (Thomas et al. 2003, Sánchez and Gens 2006): i) the main part of the water that enters the bentonite is adsorbed into the micro-pores, ii) this implies that the particles swell, and if the bentonite is restrained, this will then reduce the size of the macro-pores, iii) this will reduce the effective hydraulic conductivity of the bentonite, since only macro-pore water is available for flow (the validity of this third point is discussed in section 4.4).

In the modeling of the FEBEX mock-up test (Sánchez and Gens 2006), this effect was considered in an approximate way by reducing the intrinsic permeability in the external zone of the barrier (until a maximum of 15% for suctions lower than 2 MPa). It was found that this model could reproduce the observed behavior in the barrier better than the operational base case model. It was also found that the case with micro-fabric evolution reached total water saturation in a long term prediction, in contrast to the cases with threshold gradient or thermo-osmosis.

Micro-fabric (or microstructure) evolution was also investigated in models of the Canadian large-scale experiments Isothermal Test (Thomas et al. 2003, see section 4.4), and the Buffer-container experiment (Thomas et al. 2009).

4 Evaluation of non-standard flow models

4.1 Introduction

The goal of the evaluation is two-fold: i) to describe the mechanisms of the suggested non-standard flow models; and ii) to assess the relevance of these models for the SR-Site calculations if they would have been included in those.

Since the flow-models are not implemented in Code_Bright, there are three potential paths that can be pursued for the evaluation of these flow models: i) modification of existing numerical tool (Code_Bright); ii) development of new devoted numerical tools; iii) use of analytical methods. The first two options have been regarded as either too complex or too far-reaching to be followed during this work. The presented evaluations have, therefore, tried to employ analytical methods and descriptions.

4.2 Threshold gradient:

The notion of a threshold gradient implies that full saturation may never be reached.

For isothermal conditions this can easily be assessed with the following observation: for a bentonite specimen with the dimension of, say, 0.1 m, a threshold gradient of 50 implies that the pressure difference over the specimen is 5 m · 10 kPa/m = 50 kPa, when the threshold is reached. For unsaturated conditions this corresponds to a negligible suction value, and the saturation degree would thereby be very close to unity.

For non-isothermal conditions, however, there may be a substantial remaining unsaturated pore volume when the threshold is reached, and a steady-state saturation profile can be calculated for a specific hydraulic gradient at the cold end. Such a calculation can be based on the analytical solutions presented by Claesson (2008). A coordinate-independent relation between saturation and temperature, i.e. S(T), can be obtained for steady-state conditions with the differential equation;

$$\frac{dS}{dT} = \frac{K_T(S,T)}{K_S(S,T)} \tag{4-1}$$

and by specifying a boundary saturation degree at the cold end ($S(T_c)=S_c$). The derivation and the details about this differential equation were presented by Claesson (2008). A saturation profile S(r) can subsequently be obtained for a specified temperature profile T(r).

The differential equation, Eq (4-1), was modified concerning three parts in order to resemble the results by Sánchez and Gens (2006) as far as possible:

i. The retention curve for which the following function was used together with the following parameter values: $P_0 = 28$ MPa; $\lambda = 0.18$; $P_1 = 1100$ MPa; $\lambda_1 = 1.1$:

$$S = \left[1 + \left(\frac{P_g - P_l}{P_0}\right)^{\frac{1}{1-\lambda}}\right]^{-\lambda} \left[1 - \frac{P_g - P_l}{P_1}\right]^{\lambda_1} \tag{4-2}$$

ii. The following permeability value at saturation was used: $k_{sat} = 1.9 \cdot 10^{-21}$ m^2

iii. A temperature dependent vapour diffusion coefficient was adopted:

The vapor diffusion is in the analytical solution described as driven by **vapor density gradients**, and the diffusion coefficient includes a saturation dependence:

$$g_{vap} = -D_v(S) \nabla \rho_v \tag{4-3}$$

In the implementation of Code_Bright, the vapor diffusion is described as driven by **vapor mass fraction gradients**, and the diffusion coefficient includes a saturation dependence, **as well as a temperature dependence**:

$$i_g^w = -\rho_g \phi (1-S) \tau D_0 \frac{(273+T)^{2.3}}{p_g} \nabla \omega_g^w \tag{4-4}$$

The vapor mass fraction gradient can be transformed to a vapor density gradient in the following way:

$$\omega_g^w = \frac{\rho_v}{\rho_a + \rho_v} \approx \frac{\rho_v}{\rho_g} \quad \rightarrow \quad \nabla \omega_g^w = \frac{d\omega_g^w}{d\rho_v} \nabla \rho_v \approx \frac{\nabla \rho_v}{\rho_g} \tag{4-5}$$

In order to have the same diffusion coefficient in the analytical solution as in the Code_Bright formulation, the following function was adopted together with the following parameter values: n=0.4; τ=0.8; $D_0 = 5.9 \cdot 10^{-6}$ m^2·Pa·s^{-1}·K$^{-2.3}$; $p_g = 10^5$ Pa:

$$D_v(S,T) = -\phi (1-S) \tau D_0 \frac{(273+T)^{2.3}}{p_g} \tag{4-6}$$

Coordinate-independent relations between saturation and temperature, i.e. S(T), are shown in Figure 4-1 (left) for the above-mentioned material models and parameter values, as well as for the temperature interval 20 – 100 °C, which corresponds to the conditions in the FEBEX mock-up. Solutions for five different cold end saturation degrees are shown: 0.8, 0.9, 0.98, 0.99 and 0.998.

The temperature profile can be defined for the assumption of a constant thermal conductivity value:

$$r(T) = r_i \left(\frac{r_o}{r_i} \right)^{\frac{T_i - T}{T_i - T_o}} \tag{4-7}$$

The inner and outer radii (r_i and r_o) of the FEBEX mock-up is 0.168 and 0.795 m, respectively. This profile is shown in Figure 4-1 (right). Saturation profiles, i.e. S(r), can be obtained for the S(T) relations shown in Figure 4-1 (left) together with the temperature profile, and are shown in Figure 4-2 (left).

The hydraulic gradient can be calculated for any point along these solutions:

$$\frac{dh}{dx} = \frac{1}{\rho g} \frac{dP}{dx} = \frac{1}{\rho g} \frac{dP}{dS} \frac{dS}{dT} \frac{dT}{dx} \tag{4-8}$$

dP/dS is the derivative of the retention curve, dS/dT is the differential equation in Eq (4-1), and dT/dx is the thermal gradient. Distributions of the hydraulic gradient are illustrated in Figure 4-2 (right) for the different saturation profiles.

It can be noted that the profile with a cold end saturation of 0.998 implies a hydraulic gradient of 65 m/m at the outer radius. This is approximately the threshold gradient used by Sánchez and Gens (2006). The hot end saturation degree of this profile is 0.65. This illustrates how a threshold gradient can stop the moisture transfer into the bentonite at non-isothermal conditions, although the hydraulic gradient is significantly higher inside the bentonite.

Relevance for SR-Site calculations

To conclude, it is the non-isothermal conditions that lead to a remaining unsaturated void-space. This effect was tested for a few thermal conditions characteristic for the KBS-3 buffer. For this the canister mid-height geometry of the buffer was chosen (inner and outer radii of 0.525 and

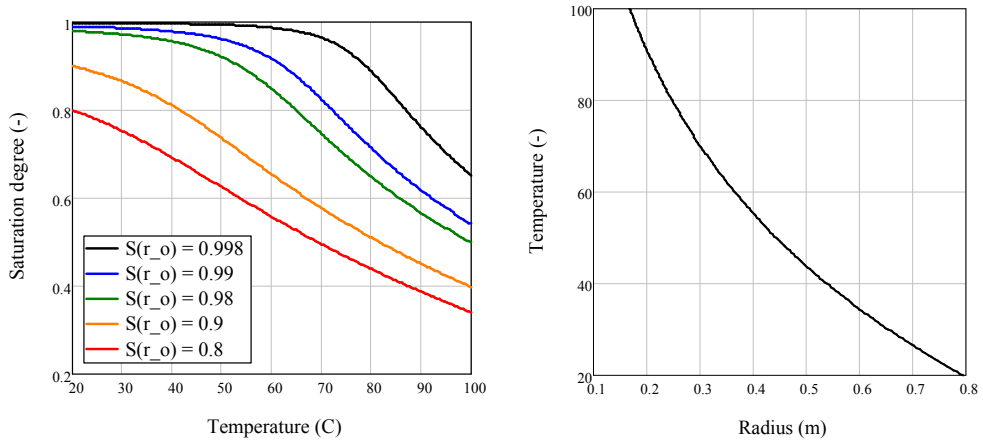

Figure 4-1. Steady-state solutions with saturation degree vs. temperature, cold end saturation is 0.8, 0.9, 0.98, 0.99, 0.998 (left).Radial profiles of temperature (right).

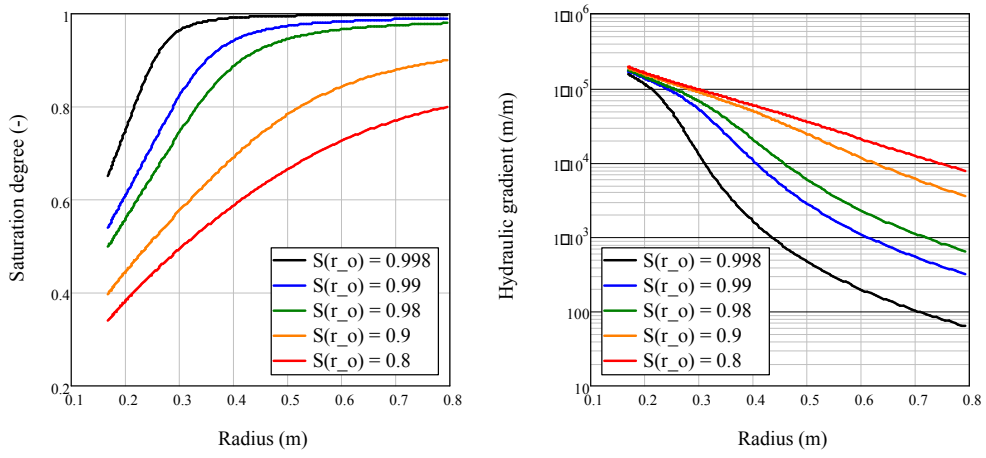

Figure 4-2. Radial profiles of saturation degree (left) and hydraulic gradient (right) for cold end saturation degree 0.8, 0.9, 0.98, 0.99 and 0.998.

0.875 m, respectively) and sets of typical inner and outer temperatures was selected for four times (10, 30, 100 and 200 years) respectively, which were derived from Hökmark et al. (2009). The material model was identical with the FEBEX model described above. For each temperature set, a S(T)-relation, and subsequently a saturation profile, was found for which the hydraulic gradient at the cold end was exactly 50 m/m. (Figure 4-3 and Figure 4-4). It can be observed, that even though this effect implies some remaining unsaturated pore volume, it can be noted that this is very small.

Even if the steady-state conditions are very close to full saturation, this does not necessarily mean that the time scale to reach these conditions is unaffected by the threshold gradient. The model results presented by Sánchez and Gens (2006) indicate, however, that the time-scale to reach steady-state with a threshold gradient is approximately the same as the time-scale to full water saturation without a threshold gradient.

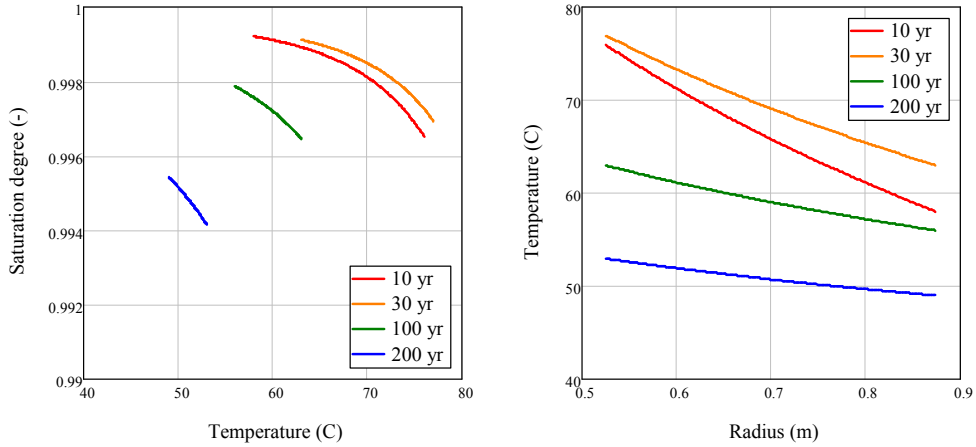

Figure 4-3. Steady-state solutions with saturation vs. temperature (left) for radial temperature profiles typical for KBS-3 canister mid-height conditions at four different times (right).

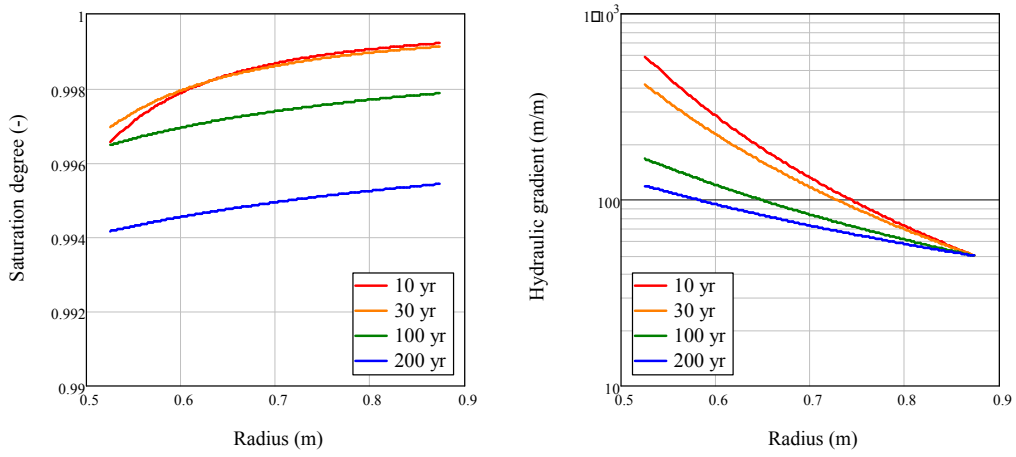

Figure 4-4. Radial profiles of saturation degree (left) and hydraulic gradient (right) for thermal conditions shown in Figure 4-3(right).

4.3 Thermo-osmosis

The notion of a thermo-osmotic flux term may imply that full saturation never is reached.

This effect can be fairly easily assessed for the FEBEX mock-up condition by following the modeling presented by Zheng and Samper (2008). This was based on a liquid flux, driven by gradients in liquid pressure, as well as in temperature:

$$q_l = -\frac{k_r k}{\mu} \nabla P_l - k_T \nabla T \tag{4-9}$$

If the vapor transport is neglected, then the steady-state condition implies that q_l is equal to zero, and from this follows that:

$$\frac{dP_l}{dT} = -\frac{k_T \nabla \mu(T)}{k_r(S) k} \tag{4-10}$$

Both sides are divided with the derivative of the inverse retention curve (dP_l/dS):

$$\frac{dS}{dT} = -\frac{k_T \nabla \mu(T)}{k_r(S) k \frac{dP_l}{dS}} \tag{4-11}$$

This is a simplification of similar steady-state solutions presented by Claesson (2008), see also Eq (4-1). The retention curve was defined on the following form:

$$S(\psi) = \frac{\left[1 + 9.1 \cdot 10^{-10} \psi\right]^{-1.1}}{\left(1 + 5 \cdot 10^{-8} \psi\right)^{1.22}}^{0.18} \tag{4-12}$$

where ψ denotes suction (defined in Pa). This curve is shown in Figure 4-5 (left).

The derivative of the inverse retention function is given as $dP_l/dS = -d\psi/dS$. The relative permeability followed the cubic law ($k_r = S_l^3$). The temperature dependence of the viscosity was defined as:

$$\mu(T) = 0.6612 (T - 229)^{-1.562} \tag{4-13}$$

where T denotes temperature (defined in K).

The value of dS/dT is in the order of $-5 \cdot 10^{-3}$ K^{-1} for the presented parameter values and for a temperature of 60 °C (Figure 4-5, left). A temperature difference between inner and outer radii of 80 °C, therefore implies a saturation difference between inner and outer radii of 0.4. An integration of the differential equation, Eq (4-11), with saturated conditions at the cold boundary, i.e. S(20°C) = 1, results in a coordinate-independent S(T)-relation. A temperature profile can be defined under the assumption of a homogenous thermal conductivity value, see Eq (4-7), and with the radial geometry of the FEBEX mock-up (Figure 4-5, right). A saturation profile can be made by combining the S(T)-relation and the temperature profile (Figure 4-5, right).

Relevance for SR-Site calculations

To conclude, as with the threshold gradient, it is the non-isothermal conditions that lead to a remaining unsaturated void space. This effect was tested for the same thermal conditions characteristic for the KBS-3 as in section 4.2. The material model was identical with the FEBEX model described above. For each temperature set, a S(T)-relation, and subsequently a saturation profile, was found for which the saturation degree as the cold end was equal to unity (Figure 4-3 and Figure 4-4). It can be observed, that this effect implies that some unsaturated pore volume will remain for a few hundred years.

Even if the steady-state conditions are fairly close to full saturation, this does not necessarily mean that the time scale to reach these conditions is unaffected by the thermo-osmosis. The model results presented by Zheng and Samper (2008) indicate, however, that the time-scale to reach steady-state with thermo-osmosis is largely the same as the time-scale to full water saturation without thermo-osmosis.

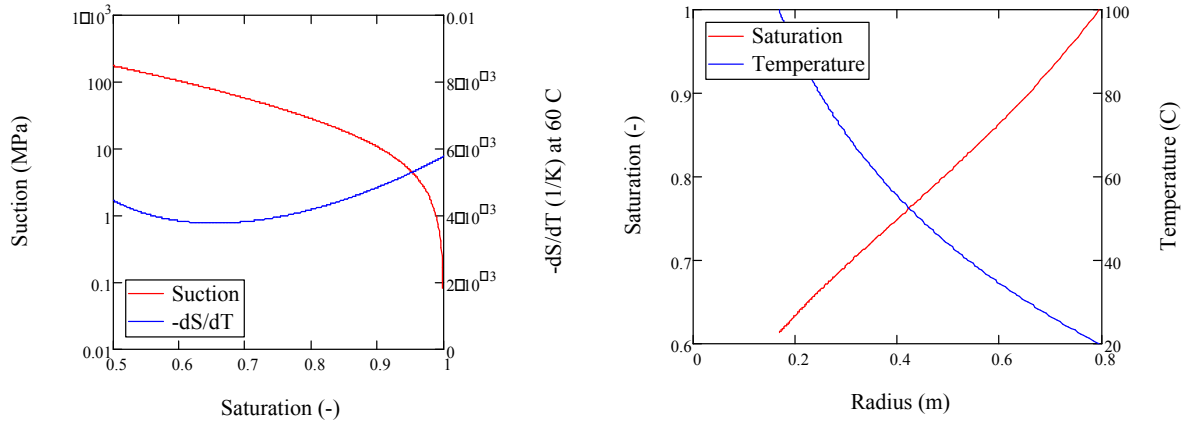

Figure 4-5. Retention curve and dS/dT derivative (left). Radial temperature distribution and steady-state saturation profile (right).

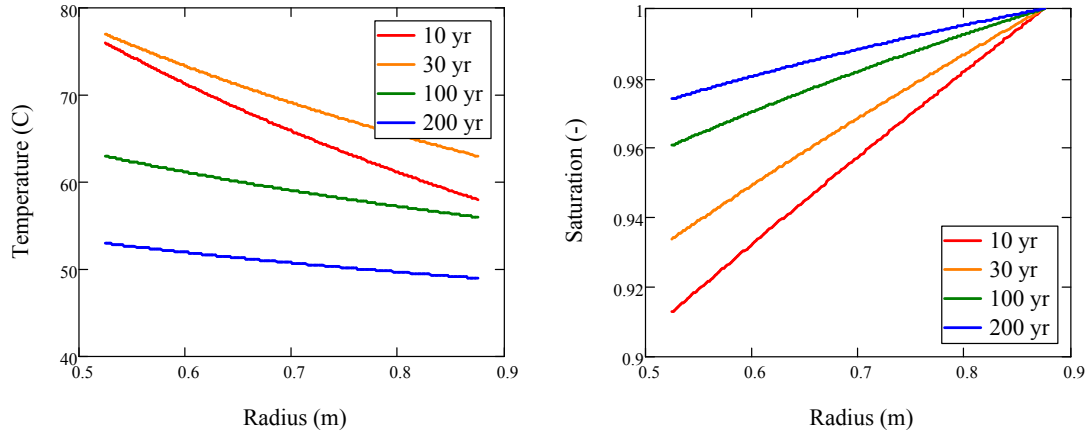

Figure 4-6. Radial temperature distribution typical for KBS-3 canister mid-height (left) and corresponding steady-state saturation profile (right).

4.4 Micro-fabric evolution

The notion of micro-structure evolution has been modeled as a reduction of the permeability value close to saturation, and this approach leads to an overall reduction in the rate of hydration. An example of an elaborate investigation of this effect was presented by Thomas et al. (2003), in a simulation of the Isothermal Test (ITT), which was one of the large-scale experiments at the Atomic Energy of Canada Limited's (AECL) underground research laboratory.

The low rate of hydration in the presented model can be illustrated through evaluation of the moisture diffusivity function, D(S):

$$D(S) = \frac{k(S)}{n \cdot \mu} \cdot \frac{dP_l}{dS} \qquad (m^2 / s) \tag{4-14}$$

where k(S)= permeability function, n=porosity, μ=viscosity, dP_l/dS=derivative of the inverse retention curve.

The used retention curve was expressed as:

$$S(\psi) = \begin{cases} 1 - 2.3 \cdot 10^{-10} \cdot [\psi - \exp(7.73 \cdot 10^{-6} \cdot \psi)] & \psi < 2.36 \cdot 10^6 \quad (Pa) \\ \dfrac{\log_{10}(\psi) - 8.23}{-3.38 \cdot e} & 2.36 \cdot 10^6 < \psi < 17 \cdot 10^6 \quad (Pa) \\ \dfrac{\log_{10}(\psi) - 8.74}{-5.08 \cdot e} & \psi > 17 \cdot 10^6 \quad (Pa) \end{cases} \tag{4-15}$$

The initial void ratio (e) was 0.56, which corresponds to a porosity (n) value of 0.36.

The hydraulic conductivity of the buffer material was first modeled with a saturation dependence following the approach proposed by Green and Corey (1971). The hydraulic conductivity is with this approach basically calculated as a sum of contributions from a number (m) of saturation classes (S_i) ranging from 0 to 1, with the first class (i=1) corresponding to S=1, and with the square of the suction value, given by Eq. (4-15), in the denominator of each term:

$$K_l(S_i) = \frac{K_s}{K_{sc}} \cdot \sum_{j=i}^{m} (2j - 1 - 2i) \cdot \psi(S_j)^{-2} \tag{4-16}$$

The saturated hydraulic conductivity (K_s) was $5 \cdot 10^{-12}$ m/s, and this value can be ensured through division with the calculated saturated conductivity value (K_{sc}) which simply is the sum in (4-16) for the first class (i=1). Note that the division with the zero suction value for S=1 leads to a singularity, and this can be handled with a factor close to unity for each S_i value. This relation is illustrated in Figure 4-7.

In order to match the experimental data, an adjusted exponential function for the hydraulic conductivity was subsequently proposed:

$$K(S) = K_l(S) \cdot [S_a + 0.06 \cdot S \cdot \exp(-100 \cdot (1 - 0.06) \cdot S)] \tag{4-17}$$

The S_a is the degree of saturation of air, and can thus be replaced by (1-S). This relation is also illustrated in Figure 4-7.

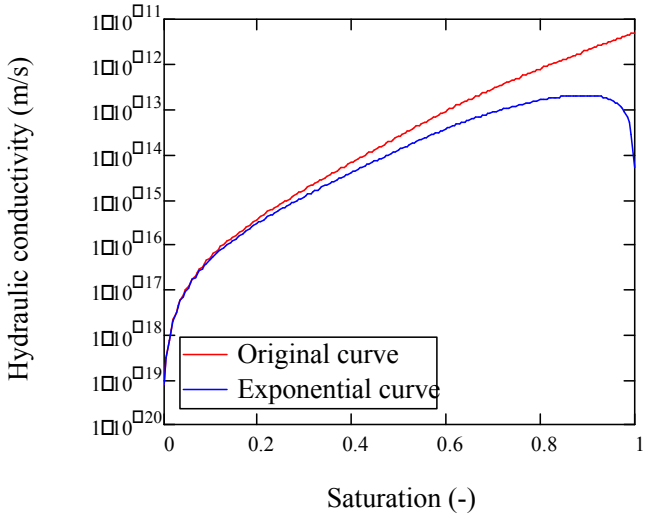

Figure 4-7. Hydraulic conductivity vs. saturation degree.

The retention curve Eq (4-15) and the adjusted hydraulic conductivity curve Eq (4-17) are shown for the relevant saturation interval in Figure 4-8, upper left. These relations were used to evaluate the moisture diffusivity function according to Eq (4-14), and this relation is illustrated in Figure 4-8, upper right. The permeability function was calculated as $10^{-7}\cdot K(S)$, due to the factor $\mu/\rho g$. The derivative of the inverse retention function was given as $dP_l/dS = -d\psi/dS$. The evaluated function indicates that the diffusivity close to saturated conditions was as low as $2\cdot10^{-10}$ m^2/s, although higher values can be noted for lower saturation degrees.

A moisture diffusivity value can easily be evaluated from the experimental data from ITT, if the hydration of the buffer material is described as a diffusion process in a cylinder (this would imply that the buffer had free access of water which may be an oversimplification to some extent).The initial and the final water content profiles (see Dixon et al. 2002) correspond to a dimensionless parameter Dt/a^2 value of approximately 0.1 for radial diffusion in a cylinder (see Crank 1975). With a radius (a) of 0.62 m and a time-scale of 6.5 years, this corresponds to a diffusivity value of $1.9\cdot10^{-10}$ m^2/s. This value is basically the same as the modeled diffusivity value close to saturated conditions.

The observed diffusivity value could be reproduced with an alternative modeling approach. Equation (4-14) implies that a permeability function can be calculated for a specified D value and defined retention curve:

$$k(S) = \frac{D[n[\sigma}{\frac{dP_l}{dS}} \qquad (4\text{-}18)$$

The following function appears to be suitable as a retention curve for simple hydration problems:

$$S(\sigma) = \left(\frac{\sigma}{P_0}\right)^{\sigma} \qquad (4\text{-}19)$$

A specified initial point (in this case S_{in}=0.86 and ψ_{in}=4 MPa) implies that there is only one independent parameter. This was calibrated in order to yield a saturated hydraulic conductivity value of $5 \cdot 10^{-13}$ m/s, as was found to be a typical value among the data from independent laboratory tests presented by Dixon et al. (2002). In this way the following parameter values were found: P_0 = 44.8 kPa and λ=0.0335. Relations for retention properties, hydraulic conductivity and diffusivity are shown in Figure 4-8, lower graphs. It can be noted that the hydraulic conductivity function display an "conventional" increasing trend for increasing degree of saturation, in contrast to the micro-fabric evolution approach. It can also be noted that the suggested retention curve display a low slope close to saturation. Such a relation is supported by the final psychrometer sensors data, and the water contents measured during the dismantling operation.

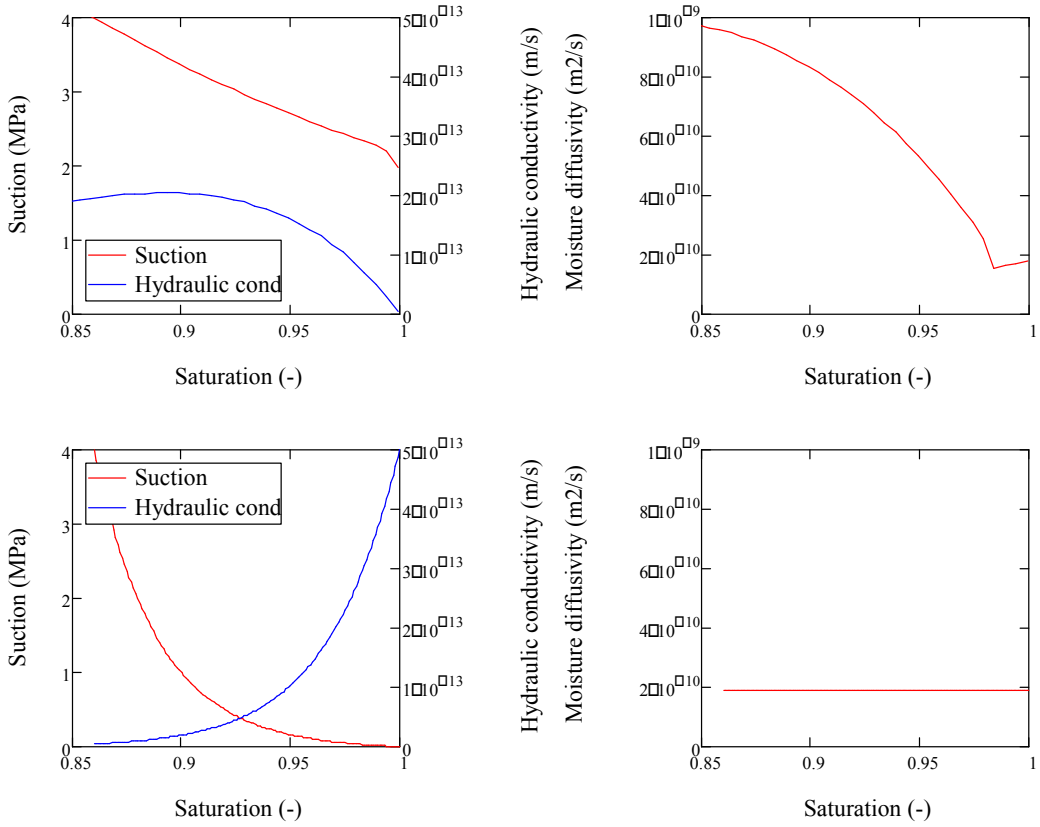

Figure 4-8. Retention curve and hydraulic conductivity relations (left) and moisture diffusivity (right). Upper graphs show data from Thomas et al. (2003), lower graphs show data from this analysis.

Relevance for SR-Site calculations

To conclude, in contrast to the threshold and the thermo-osmosis there is no effect with a remaining unsaturated void space in the case of micro-structure evolution, but rather a reduced rate of water uptake. The main cause for this is the reduced relative permeability relation.

The physical basis for such an approach would be that only macro-pore water is available for flow (Thomas et al. 2003). It is however unclear why the effective conductivity value, Eq. (4-17), close to saturation would be orders of magnitude lower than the measured hydraulic conductivity.

Still, the low evaluated diffusivity value seems to coincide with similar values for low density MX-80 (see Åkesson 2013), and this seems to support the notion that the Isothermal Test indeed displayed a low hydration rate. An overall water content of 18-22%, would correspond to a clay water content of 36 – 44% given the 50:50 sand-bentonite mixture. According to the analysis presented by Börgesson et al. (2013) this suggests that the mechanism behind the slow hydration rate could be that vapour diffusion limits the moisture transfer.

A simple assessment of the consequences of the micro-structure evolution for the SR-Site calculations can thus tentatively be made by comparing the moisture diffusivity value typical for the MX-80 buffer with the lower diffusivity values mentioned above.

The material model adopted for buffer hydration calculations in SR-Site, see Åkesson et al. (2010) (homogenized approach and retention curves using the extended van Genuchten function) was used to calculate the corresponding moisture diffusivity functions with Eq. (4-14) which are shown in Figure 4-9. These functions display a level of approximately $7 \cdot 10^{-10}$ m^2/s. This can first and foremost be compared with the empirical diffusivity values presented by Åkesson (2013), which did not exceed the level of $5 \cdot 10^{-10}$ m^2/s for MX-80 at buffer dry densities. This can therefore indicate a minor underestimation of the buffer hydration time-scale in SR-Site. If the SR-Site calculations would have been performed with the lowest empirical diffusivity values (~ $2 \cdot 10^{-10}$ m^2/s) then this would lead to a 3.5 times longer time for buffer-hydration (at wet rock conditions)

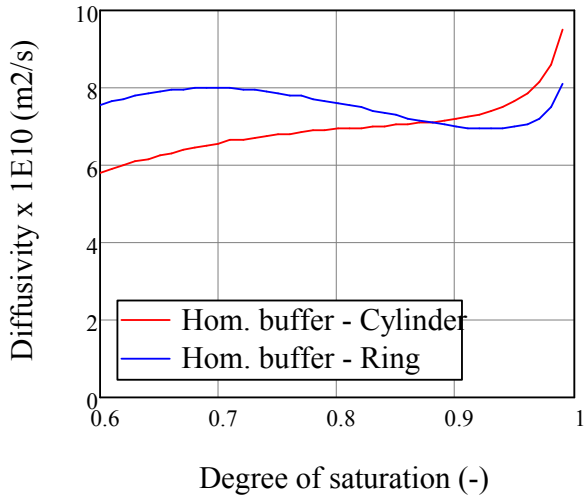

Figure 4-9. Moisture diffusivity function based on the material model for buffer hydration calculations.

5 Other uncertainties

5.1 Introduction

During the course of the work with the presented analysis, it was noticed that a few other conceptual uncertainties also deserved a thorough evaluation. This concerned: i) natural convection in pellets-filled slots, and ii) the temperature dependence of the retention properties. These evaluations are presented in the following subsections.

5.2 Natural convection in pellets-filled slots

5.2.1 Background

The water saturation process and the time-scale of the buffer hydration was analysed by Åkesson et al. (2010). Among the analysed models, those with low inflow of water (low rock permeability) exhibited significant moisture redistribution, and this was also the case in models with no water inflow (dry rock scenario). The steady-state conditions and the time-scale to reach this state are to some extent determined by the flow coefficients. For dry rock conditions the most important transport process is the diffusion of vapour, and this was the only means to transfer moisture from hot to cold parts in the presented models. The potential contribution of natural convection to a more pronounced moisture redistribution has therefore been identified as a conceptual uncertainty for the evolution of the re-saturation. The result from a first assessment of this process is presented in this section.

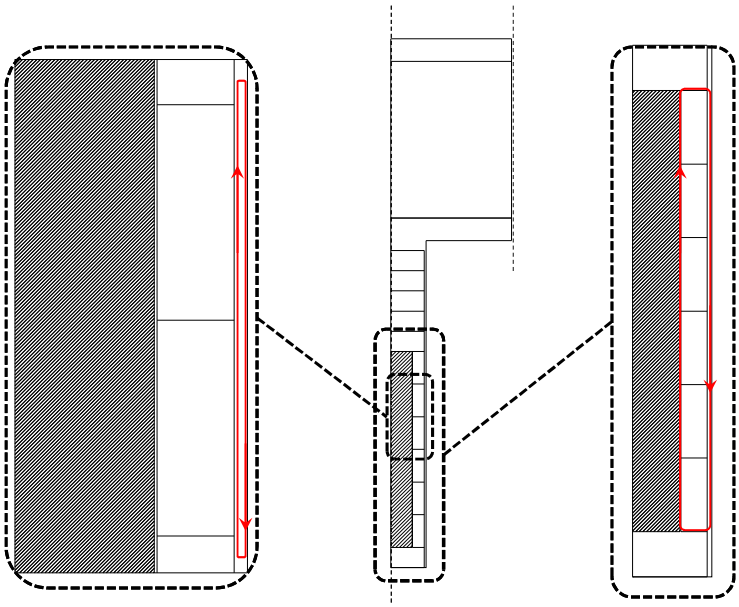

Figure 5-1. Suggested modes of natural convection in pellets-filled slot. In outer slot only (left) and in inner and outer slot (right).

Natural convection is a mechanism of heat transfer, involving the motion of a fluid (air in this case), which is the result of density differences, which in turn are caused by the exchange of heat. As a starting point, two modes of such air motions were suggested (Figure 5-1): either through a loop in the outer pellets-filled slot; or through a loop in both the inner and the outer slots, as well as through the joints between the bentonite blocks.

The complexity of the problem would be enhanced if moisture redistribution was included in these modes of air movement. Still, it is possible that the condition for the occurrence of natural conditions can be estimated with these simple descriptions.

5.2.2 Assessment of occurrence of natural convection

The evaluation below was based on the description of natural convection in a two-dimensional rectangular enclosure with a porous medium and isothermal side walls, presented by Nield and Bejan (2006). The geometry is shown in Figure 5-2 (left).

The Rayleigh number (Ra) is a dimensionless number of significance for natural convection and is equal to the product of the Grashof and the Prandtl number. For the geometry in question it can be expressed as:

$$Ra = \frac{g\beta K H \Delta T}{\nu \alpha_m} \quad (5\text{-}1)$$

where g = gravity; β = thermal expansion coefficient; K = permeability; H = height of enclosure, ΔT = temperature difference between sides; ν = kinematic viscosity; α_m = thermal diffusivity of porous medium. It can be noted that the main uncertainty among these quantities is the K value.

A second dimensionless number of importance for natural convection is the Nusselt number (Nu), which is the ratio between total heat transfer, and conductive heat transfer. For the geometry in question a substantial amount of data (theoretical as well as experimental) has been used to adopt the following relation between Nu, Ra and the ratio of the dimensions of the enclosure:

$$Nu = 0.577 \frac{L}{H} \sqrt{Ra} \quad (5\text{-}2)$$

where L = width of the enclosure (see Figure 5-2, right).

If the point on which Nu equals unity (i.e. $Ra(L/H)^2 = 3$), is regarded as the condition for natural convection to occur, then this can be used to calculate the maximum height of the slot (H_{max}) as a function of the permeability:

$$H_{max}(K) = \frac{L^2 g \beta K \Delta T}{3 \nu \alpha_m} \quad (5\text{-}3)$$

It should be mentioned that this may be a conservative approach since it was also stated by Nield and Bejan (2006) that $\sqrt{Ra} >> H/L$ in order to get a distinct vertical boundary layers, and that this is a requirement for this type of convection.

A graph is shown (Figure 5-3) for a case with the following parameter values: L = 0.05 m (and 0.1 m); g = 9.8 $m \cdot s^{-2}$; $\beta = 0.003\ K^{-1}$; $\Delta T = 5\ °K$; $\nu = 1.9 \cdot 10^{-5}\ m^2 \cdot s^{-1}$; $\alpha_m = 3.3 \cdot 10^{-7}\ m^2 \cdot s^{-1}$. The thermal diffusivity value was based on a thermal conductivity value of 0.4 $W \cdot m^{-1} \cdot K^{-1}$. The thermal expansion and the viscosity for air were adopted for a temperature of 60 °C. These values, and the adopted temperature difference, were derived from Hökmark et al. (2009).

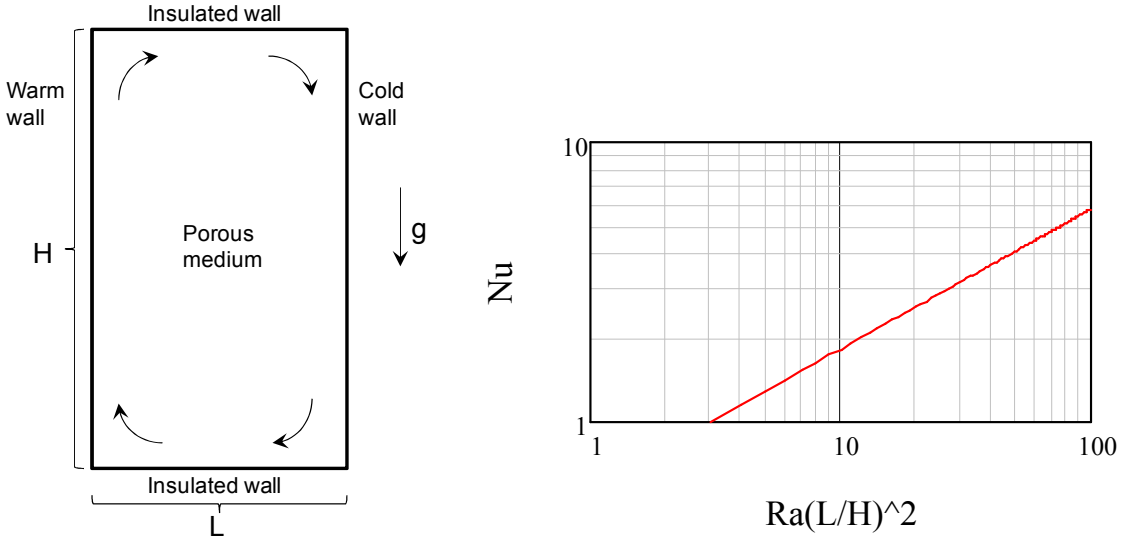

Figure 5-2. Rectangular porus medium between heated side walls, left; illustration of Eq (5-2), right (after Nield and Bejan 2006).

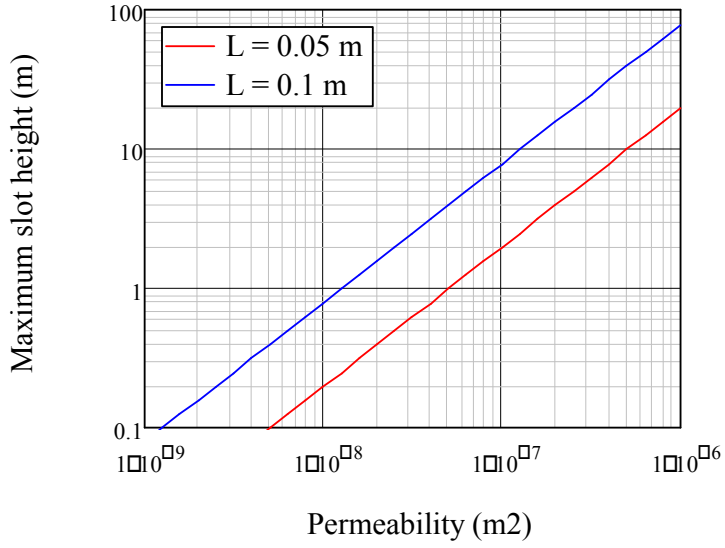

Figure 5-3. Maximum height with sustained natural convection.

These graphs thus show the maximum height with sustained natural convection. A lower height would imply a Nu-value higher than unity, and thus a convective heat transfer. Graphs are shown for two values of the slot width: 0.05 m, which represents the width of the pellets-filled slot, and the double value of 0.1 m. This latter analysis can be regarded as an estimate for the case with motion in both inner and outer slots, since the downward movement in this case can occupy the entire width of the pellets-filled slot, rather than only half the width.

5.2.3 Concluding remarks

A key property for natural convection to occur in the pellets-filled slot is apparently the (gas) permeability of pellets. This property has with the author's knowledge not been quantified experimentally. Still, an estimate can be made for "cleaned gravel" for which a permeability interval of 10^{-9} to 10^{-7} m^2 has been given (Bear 1972). If 10^{-7} m^2 is used as a conservative value for pellets, then for L=0.05 m the maximum height is 2 m, which can be regarded as fairly low in comparison to the lengths of the canister and the deposition hole. For L= 0.1 m, however, the maximum height is 8 m, which is higher than the canister. With the available information, it therefore appears to be more probable to have a sustained natural convection through both the inner and the outer slot, than through only the outer.

The presented assessment only addresses the condition for convective heat transport to occur, and hence the overall transport of air. An estimation of the actual gas flow rates, and their contribution to the moisture redistribution, appears to be far more complex. A convective transfer of vapour from hot to cold parts should imply that the equilibration of vapour pressure is more far-reaching than in the case with only diffusion of vapour. The major temperature difference between the hot parts close to the canisters and the cold parts in the tunnel ceiling, which will be prevalent during the first decades, also implies a major difference of the saturated vapour pressure in these parts. And this difference defines how far the moisture redistribution potentially can proceed. The tunnel volumes will to a large extent be backfilled with pellets which means that the accessible air-filled volumes of the backfill are substantial in comparison to the water volume of the installed buffer. Finally, the water retention properties of the bentonite describe a relation between the water content and the relative humidity. A completely equilibrated vapour pressure would therefore imply a major dehydration of the buffer (Figure 5-4). How much further the actual moisture redistribution will proceed in comparison to the case with only vapour diffusion should depend on the flow rates of the natural convection. Water uptake in the pellets-filled slot may have a retarding influence on this moisture transfer. However, experimental results from the Bastu-project (Birgersson and Goudarzi, 2013) showed that only a minor fraction of the vapour passing through the investigated pellets fillings was adsorbed by the pellets.

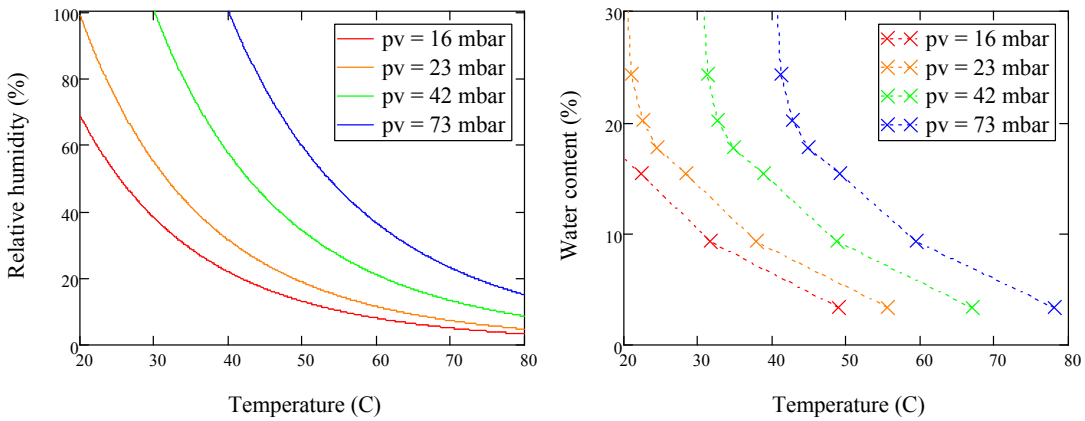

Figure 5-4. Relations between RH and temperature (left) and water content and temperature (right) at equilibrated vapour pressures. Right graph based on water retention data for free swelling conditions and for an initial water content of 17% (Dueck, 2004).

5.3 Temperature dependence of retention properties

5.3.1 Background

Experimental data by Dueck and Nilsson (2010) and Villar and Gòmez-Espina (2007) show that the retention properties are temperature dependent. The general trend is that RH increases (suction decrease) with increasing temperature. Data by Kahr et al. (1990) suggest that this effect may be more significant for Ca dominated bentonite than for a Na dominated bentonite. This chapter describes the results from an assessment of this effect.

5.3.2 Assessment of the effect of temperature dependence

Kahr et al. (1990) presented a number of thermodynamic properties for systems with water and Na- and Ca-bentonites, i.e. MX-80 and Montigel, respectively.

The enthalpy change ($\overline{h_w} - h_w^\circ$, where $\overline{h_w}$ and h_w° are the partial specific enthalpy of water in the bentonite and the enthalpy of the pure water) was evaluated from measured enthalpies of immersion. The experimental data could be described as a function for the influence of the water content on the following form:

$$\left[\overline{h_w} - h_w^\circ\right] = (B - 2Cw)A \cdot \exp(-Bw - Cw^2) \qquad (J/g) \tag{5-4}$$

For MX-80 bentonite the following parameter values were found: A=47.18; B=8.53; C=29.28, while for Montigel the following were found: A=90.14; B=8.66; C= 33.54.

The difference between the free energies of water in the water-bentonite system and pure water were obtained from swelling pressure measurements, and the data could be described as a function for the influence of the water content on the following form:

$$\left[\overline{g_w} - g_w^\circ\right] = \exp(a - b \cdot w) \qquad (J/g) \tag{5-5}$$

For MX-80 bentonite the following parameter values were found: a=6.00 and b=17.8, while for Montigel the following were found; a=6.66 and b=18.6 (note that 1 J/g is equivalent to 1MPa for a partial specific volume of water of 10^{-3} m^3/kg) An alternative parameter set was obtained by Dueck (2007) for MX-80 with an initial water content of 10%: a=6.3 and b=16. The following parameter values were fitted to retention data for Febex bentonite presented by Villar (2002): a=8 and b=22. All four relations are illustrated in Figure 5-4. It can be noted that the suction values presented by Kahr et al. (1990) are significantly lower than the corresponding data by Dueck (2007) and Villar (2002).

Finally, Kahr et al. (1990) provided the following relation between the enthalpy change, the difference in free energy, the absolute temperature (T), and the entropy change ($\overline{s_w} - s_w^\circ$):

$$\left[\overline{h_w} - h_w^\circ\right] = \left[\overline{g_w} - g_w^\circ\right] - T \cdot \left[\overline{s_w} - s_w^\circ\right] \tag{5-6}$$

The entropy changes are shown as functions of the water content in Figure 5-5. Both graphs are based on the original enthalpy data by Kahr et al. (1990). The left graph is also based on the original free energy data by Kahr et al. (1990). The right graph, however, is based on the retention data presented by Dueck (2007) and Villar (2002). It can be noted that the difference

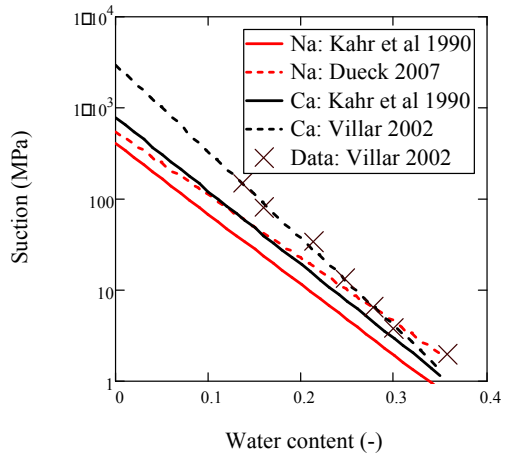

Figure 5-4. Retention curves and experimental data (FEBEX) for unconfined conditions.

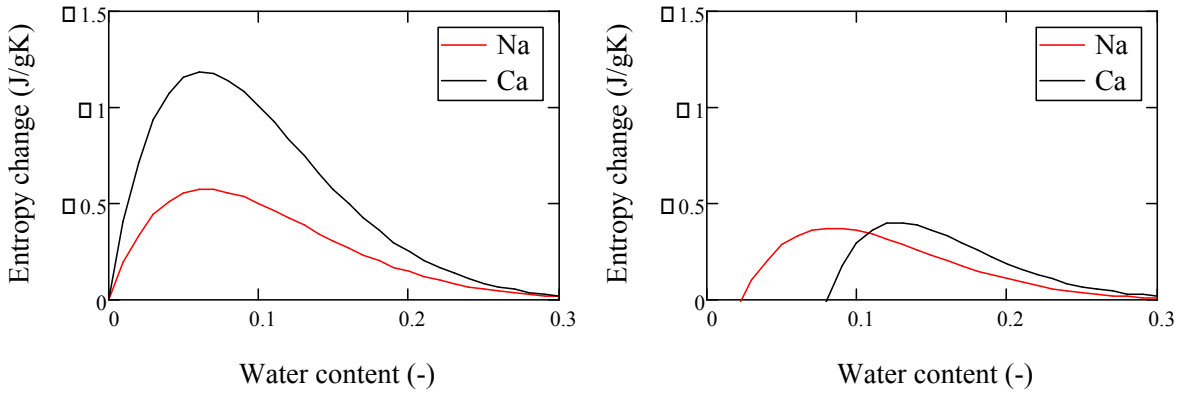

Figure 5-5. Entropy change as a function of water content according to data by Kahr et al. (1990) (left); according to entalpy data by Kahr et al. (1990), and retention data according to Dueck (2007) and Villar (2002), respectively (right).

between the two relations (for Na- and Ca-bentonite, respectively) in the right graph appears to be smaller than the corresponding differences in the left graph.

The influence of the temperature on the retention properties for free swelling conditions was described by Birgersson et al. (2010) with the following expression:

$$\Delta_{free}(w,T) \approx \Delta_{free}(w,T_0) - \frac{\Delta s(w)\,\Delta T}{\nu} \qquad (5\text{-}7)$$

The entropy change $\Delta s(w)=s_{clay}(w)-s_{ref}$ corresponds to the $(\overline{s_w} - s_w^{\circ})$ described above. The temperature difference ΔT was defined as $T-T_0$. With ν is here meant the specific volume of water (10^{-3} m^3/kg) due to the used unit for Δs (J/gK) in Eq (5-6).

This description of the temperature dependence was compared with experimental retention curves for MX-80 obtained with the sorption balance technique at two different temperatures (20 and 50 °C) reported by Dueck and Nilsson (2010). Two calculations were made for each temperature: either with data solely from Kahr et al. (1990), or with enthalpy data by Kahr et al. (1990) and

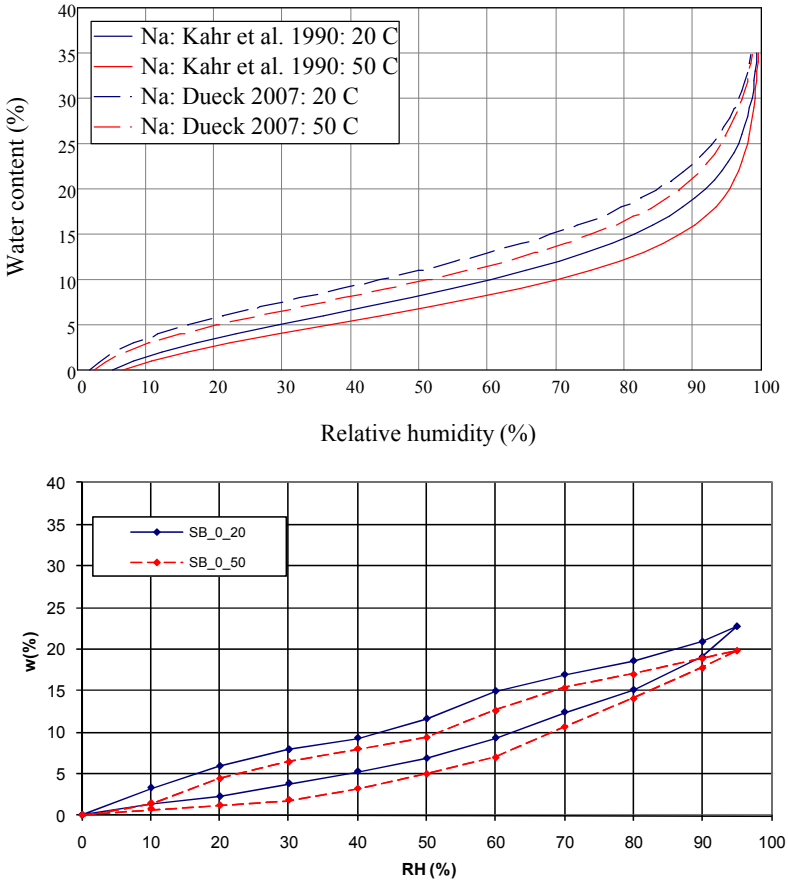

Figure 5-6. Retention curves for MX-80 at 20 and 50□C. Calculated with Eq (5-7) (upper graph) and determined with the sorption balance method and zero initial water content (lower graph).

retention data presented by Dueck (2007). The results are shown in Figure 5-6. As expected by the entropy change data, the latter data set implies a smaller temperature dependence than the former, and this is apparently more in agreement with the experimental retention curves. Still, it should be observed that the retention curve by Dueck (2007) were obtained for an initial water content of 10%, whereas the adsoption data by Dueck and Nilsson (2010), as well as Kahr et al. (1990) were obtained for a zero initial water content.

The relation between the suction for confined conditions and for free swelling conditions can be described:

$$\Delta_{conf}(w,T) \approx \Delta_{free}(w,T) + \alpha P \qquad (5\text{-}8)$$

Where P is the pressure and α is a compressibility factor. The value of the parameter α is usually assumed to be equal to unity, even though other values have been reported.

Equations (5-7) and (5-8) can be combined in order include both a temperature dependence and a pressure dependence:

$$\rho_{conf}(w,T) \approx \rho_{free}(w,T_0) \cdot \frac{\Delta s(w) \cdot (T - T_0)}{\rho} \cdot P \qquad (5\text{-}9)$$

This relation is analyzed for the case with a given pressure level (7 MPa), a zero suction value, and for temperatures between 20 and 100 °C. Such isobars are shown in Figure 5-7 for all entropy change relations shown in Figure 5-5. These relations could in principle constitute saturation profiles for which the hydration stops, and therefore corresponds to the saturation profiles in Figure 4-1 and Figure 4-5. It can be noted that the unsaturated void space would be fairly small in the cases based on the retention data by Dueck (2007) and Villar (2002), and significantly larger in the cases with the original entropy changes presented by Kahr et al. 1990.

The consequences of this effect would be even smaller for the thermal conditions in KBS-3. A typical temperature at the outer and inner radii of the canister mid-height section was 58 and 76 °C after ten years. This interval would result in a range in water content from 26.4 to 25.9 %, according to the results in Figure 5-7 for the case with Na bentonite and retention data by Dueck (2007).

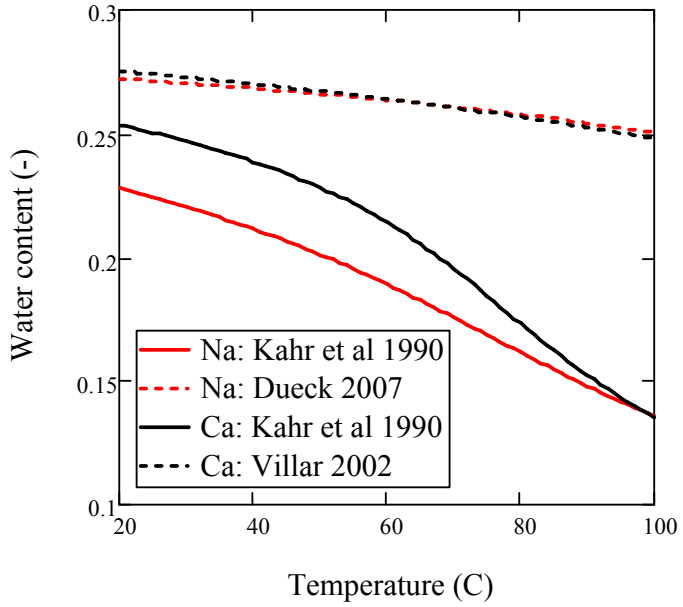

Figure 5-7. Zero suction water content as a function of temperature at P= 7 MPa.

5.3.3 Concluding remarks

The presented analysis indicates that the effects of the temperature dependence of the retention properties are very small, especially for the temperature intervals typical for KBS-3. Still, it should be observed that the presented calculations are based on measurements of enthalpies of immersion which were performed more than 25 years ago.

6 References

Alonso E E, Alcoverro J, 2005. Decovalex III project. Modelling of FEBEX In-Situ test. Task 1 Final report. SKI Report 2005:20.

Alonso E E, Gens A, Josa A, 1990. A constitutive model for partially saturated soils. Géotechnique **40**, No. 3, 405-430.

Alonso E E, Alcoverro J, Coste F, Malinsky L, Merrien-Soukatchoff V, Kadiri I, Nowak T, Shao H, Nguyen T S, Selvadurai A P S, Armand G, Sobolik S R, Itamura M, Stone C M, Webb S W, Rejeb A, Tijani M, Maouche Z, Kobayashi A, Kurikami H, Ito A, Sugita Y, Chijimatsu M, Börgesson L, Hernelind J, Rutqvist J, Tsang C-F, Jussila P, 2005. The FEBEX benchmark test: case definition and comparison of modelling approaches. International Journal of Rock Mechanics & Mining Sciences, 42**,** 611–638.

Bear J, 1972. Dynamics of fluids in porous media. Dover Publications, New York.

Birgersson M, Goudarzi R, 2013. Studies of vapor transport from buffer to tunnel backfill (sauna effects). SKB R-13-42, Svensk Kärnbränslehantering AB.

Birgersson M, Karnland O, Nilsson U, 2010. Freezing of bentonite. Experimental studies and theoretical considerations. SKB TR-10-40. Svensk Kärnbränslehantering AB.

Börgesson L, Åkesson M, Hernelind J, 2013. 3.2 Analysis of risks and consequences of uneven wetting in a dry deposition hole**.** SKBdoc 1415878, version 1.0, Svensk Kärnbränslehantering AB.

Claesson J, 2008. Selected models for key processes in a nuclear waste repository. Temperature field – bentonite drying/resaturation. SKI Report 2008:47.

Crank J, 1975. The mathematics of diffusion, 2nd ed.; Oxford University Press, Oxford.

DeGroot S R, Mazur P, 1984. Non-Equilibrium Thermodynamics. Dover Publications, New York.

Dixon D, Chandler N, Graham J, Gray M N, 2002. Two large-scale sealing tests conducted at Atomic Energy of Canada's underground research laboratory: the buffer–container experiment and the isothermal test. Can. Geotech. J. **39**: 503–518.

Dueck A, 2004. Hydro-mechanical properties of a water-unsaturated sodium bentonite. Laboratory study and theoretical interpretation. Ph. D. Thesis, Lund University.

Dueck A, 2007. Results from suction controlled laboratory tests on unsaturated bentonite – verification of a model. In: Schanz, T. (Ed.), Experimental Unsaturated Soil Mechanics, Springer Proceeding in Physics, 112, 329-335.

Dueck A, Nilsson U, 2010. Thermo-Hydro-Mechanical properties of MX-80. Results from advanced laboratory tests. SKB TR-10-55, Svensk Kärnbränslehantering AB.

Gens A, Sánchez M, Guimarães, L Do N, Alonso E E, Lloret A, Olivella S, Villar M V, Huertas F, 2009. A full-scale in situ heating test for high-level nuclear waste disposal: observations, analysis and interpretation. Géotechnique, vol 59, no. 4, pp. 377-399.

Green R E, Corey J C, 1971. Calculation of hydraulic conductivity: a further evaluation of some predictive methods. In Proc. of the Soil Society of America, Vol. 35, pp. 3-8.

Hökmark H, Sundberg J, Kristensson O, Lönnqvist M, Hellström G, 2009. Strategy for thermal dimensioning of the final repository for spent nuclear fuel. SKB R-09-04, Svensk Kärnbränslehantering AB.

Kahr G, Kraehenbuehl F, Stoeckli H F, Müller-Vonmoos M, 1990. Study of the water-bentonite system by vapour adsorption, immersion calorimetry and X-ray techniques: II. Heats of immersion, Swelling pressures and Thermodynamic properties. Clay Minerals v.25, 499–506.

Martin P L, Barcala J M, 2005. Effects of over-heating on the performance of the engineering clayed barriers of the mock-up test. Advances in Understanding Engineered Clay Barriers (2005) 391-412.

Mitchell J K, 1993. Fundamentals of soil behavior. John Wiley & Sons, Inc. New York.

Nield D A, Bejan A, 2006. Convection in Porous Media. Third Edition. Springer. New York.

Sánchez M, Gens A, 2006. FEBEX Project, Final report, Final report on thermo-hydro-mechanical modelling. ENRESA publicación técnica 05-2/2006. Madrid.

Sánchez M, Villar M V, Lloret A, Gens A, 2007. Analysis of the expansive clay hydration under low hydraulic gradient. In: Schanz, T. (Ed.), Experimental Unsaturated Soil Mechanics, Springer Proceeding in Physics, 112, 309-318.

Thomas H R, Clear P J, Chandler N, Dixon D, Mitchell H P, 2003. Water infiltration into a large-scale in situ experiment in an underground research laboratory. Géotechnique, vol 53, no. 2, pp. 207-224.

Thomas H R, Clear P J, Dixon D, Mitchell H P, 2009. The coupled thermal-hydraulic-mechanical behavior of a large-scale in situ heating experiment. Géotechnique, vol 59, no. 4, pp. 401-413.

Tsang C-F, Stephansson O, Jing L, Kautsky F, 2009. DECOVALEX Project: from 1992 to 2007. Environ Geol vol 57, pp. 1221-1237.

Villar MV, 2002. Thermo-hydro-mechanical characterization of a bentonite from Cabo de Gata. A study applied to the use of bentonite as sealing material in high level radioactive waste repositories. ENRESA publicación técnica 04/2002. Madrid.

Villar M V, Gòmez-Espina R, 2007. Retention Curves of Two Bentonites at High Temperature. In: Schanz, T. (Ed.), Experimental Unsaturated Soil Mechanics, Springer Proceeding in Physics, 112, 267-274.

Zheng L, Samper J, 2008. A coupled THMC model of FEBEX mock-up test. Physics and Chemistry of the Earth, **33**, 508-515.

Åkesson M, Kristensson O, Börgesson L, Dueck A, Hernelind J, 2010. THM modelling of buffer, backfill and other system components. Critical processes and scenarios. SKB TR-10-11, Svensk Kärnbränslehantering AB.

Åkesson M, 2013. 1.4 Bentonites other than MX-80. Clay Technology. SKBdoc 1415875, version 1.0, Svensk Kärnbränslehantering AB.